SPECTRUM OF ENGINEERING SCIENCES
ISSN (E) 3007-3138 (P) 3007-312X VOLUME 4, ISSUE 3, 2026

HYBRID NANOCOMPOSITE ELECTRODES INTEGRATING METAL OXIDES, MXENES, GRAPHENE, AND CONDUCTIVE POLYMERS FOR HIGH-ENERGY-DENSITY SUPERCAPATTERY SYSTEMS

Muhammad Junaid Afzal*[1], Nasir Mehmood[2]

[1]*Riphah International University Islamabad (Lahore Campus), Pakistan*
[2]*Department of Chemistry, University of Gujrat*

junaid.afzal.phy@outlook.com[1] nasirsaddeqi@gmail.com[2]

DOI: https://doi.org/10.5281/zenodo.23828342

Keywords
Supercapattery, Hybrid Nanocomposite Electrodes, MXenes, Transition Metal Oxides, Graphene, Conductive Polymers, Energy Density, Pseudocapacitance

Article History
Received: 01 January 2026
Accepted: 16 March 2026
Published: 31 March 2026

Copyright @Author
Corresponding Author: *
Muhammad Junaid Afzal

Abstract

The global transition toward sustainable energy grids and electrified transportation has intensified the demand for advanced electrochemical energy storage (EES) technologies capable of concurrently delivering high energy density, rapid power capability, and long-term cycling stability. Supercapatteries, as asymmetric battery-supercapacitor hybrid devices, have emerged as promising solutions to bridge the performance gap between conventional electrochemical double-layer capacitors (EDLCs) and rechargeable lithium-ion batteries. This study examines the design, synthesis, interfacial kinetics, and electrochemical performance of multi-component hybrid nanocomposite electrodes integrating transition metal oxides (TMOs), MXenes, graphene, and conductive polymers (CPs) for high-energy-density supercapattery systems. The synergistic roles of each component are critically analyzed: TMOs provide high theoretical Faradaic capacity, MXenes contribute metallic conductivity and intercalation pseudocapacitance, graphene offers exceptional surface area and mechanical flexibility, while conductive polymers supply additional pseudocapacitance and act as elastic binders. Advanced synthesis strategies including hydrothermal crystallization, in-situ polymerization, and self-assembly are evaluated for constructing integrated heterostructures with optimized interfacial coupling. Key electrochemical performance metrics, charge storage mechanisms, and power-law kinetic analysis are systematically discussed. System-level integration considerations including charge balancing, voltage window expansion, and impedance optimization are addressed. Despite remarkable progress, challenges remain regarding MXene oxidation, interfacial delamination, and synthesis complexity. Emerging strategies such as high-entropy MXenes, 3D aerogel architectures, covalent organic framework integration, and AI-driven design are highlighted as promising pathways for next-generation supercapattery electrodes.

1. INTRODUCTION

The global transition toward sustainable energy grids and electrified transportation has intensified the demand for advanced electrochemical energy storage (EES) technologies capable of concurrently delivering high energy density, rapid power capability, and long-term cycling stability (Priyadharshini et al., 2026). Conventional electrochemical energy storage technologies are fundamentally divided between electrochemical

double-layer capacitors (EDLCs) and rechargeable batteries. EDLCs store charge through non-Faradaic electrostatic ion accumulation at the electrode/electrolyte interface, delivering high power densities (> 10 kW kg^{-1}) and long operational lifespans ($> 10^5$ cycles). However, their low gravimetric energy density (0.5–10 Wh kg^{-1}) limits their use in applications requiring sustained power delivery (Basirun et al., 2021). Conversely, lithium-ion batteries rely on solid-state Faradaic bulk diffusion mechanisms, achieving high specific energy densities (125–200 Wh kg^{-1}) at the expense of power delivery (< 1 kW kg^{-1}), charge-discharge rates, and cycle life due to strain-induced phase transformations (Gusain et al., 2021).

To bridge this performance gap, the "supercapattery" (also designated as a battery-supercapacitor hybrid device) has emerged as an asymmetric storage system. Supercapatteries integrate a high-capacity Faradaic battery-type or pseudocapacitive positive electrode with a high-rate non-Faradaic capacitive negative electrode within a single cell (Afreh et al., 2025). This hybrid design leverages both rapid interfacial electrostatic adsorption and reversible multi-electron Faradaic redox reactions. Consequently, supercapatteries routinely achieve energy densities ranging from 20 to 100 Wh kg^{-1} while maintaining power densities exceeding 5000 W kg^{-1} (Gür, 2018).

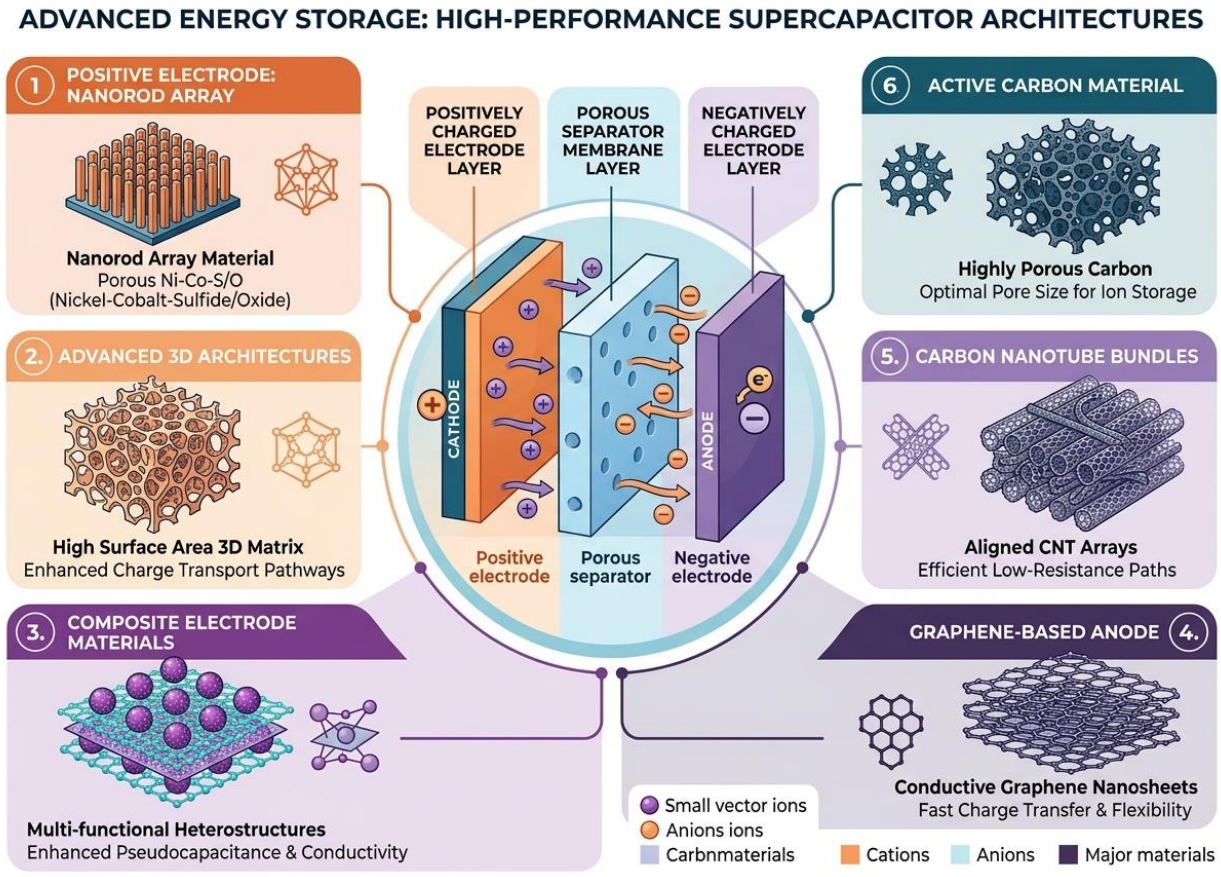


Figure 1. Schematic illustration of multi-component active electrode architectures and interfacial ion transport pathways in advanced energy storage systems.

Table 1: Comparative Overview of Primary Electrochemical Energy Storage Systems

Metric / Feature	Electrochemical Double-Layer Capacitors (EDLCs)	Supercapattery Systems	Rechargeable Lithium-Ion Batteries
Primary Charge Mechanism	Non-Faradaic physical ion adsorption	Combined Faradaic redox & non-Faradaic electrostatic	Bulk Faradaic intercalation & phase conversion
Energy Density (Wh kg^{-1})	$0.5 - 10$	$20 - 100$	$125 - 200$
Power Density (W kg^{-1})	$> 10{,}000$	$\geq 5{,}000$	$< 1{,}000$
Charge/Discharge Time	Seconds	Seconds to Minutes	Hours
Cyclic Lifespan (Cycles)	$> 100{,}000$	$5{,}000 - 10{,}000+$	$1{,}000 - 2{,}000$
Primary Electrode Limitation	Limited electrostatic surface area	Interfacial transport kinetics & restacking	Volumetric lattice strain & sluggish kinetics

The ultimate performance of a supercapattery system is governed by the structural, electronic, and electrochemical properties of its active electrode materials. Single-component materials possess intrinsic performance trade-offs:

- Transition metal oxides (TMOs) offer high theoretical Faradaic capacity, but suffer from low intrinsic electronic conductivity (10^{-6} to 10^{-2} S cm^{-1}) and structural degradation caused by volumetric swelling during charge/discharge cycles (Detka, K., & Górecki, 2023).
- Two-dimensional (2D) carbon structures like graphene possess exceptional theoretical specific surface area (2630 m^2 g^{-1}) and metallic conductivity (10^6 S cm^{-1}), but tend to restack via strong Van der Waals forces, reducing their accessible surface area down to ~ 705 m^2 g^{-1}.
- 2D transition metal carbides/nitrides/carbonitrides (MXenes) exhibit metallic electrical conductivity (2.4×10^4 S cm^{-1}), hydrophilic surface terminations ($-O$, $-OH$, $-F$, $-Cl$), and fast cation intercalation pseudocapacitance, but suffer from irreversible restacking and self-oxidation (Solyali et al., 2022).
- Conductive polymers (CPs) such as polyaniline (PANI) and polypyrrole (PPy) supply high specific capacitance through fast Faradaic doping/dedoping, but undergo mechanical breakdown during ion cycling (Márquez et al., 2023).

To address these material limitations, multi-component hybrid nanocomposite electrodes integrating TMOs, MXenes, graphene, and CPs have been developed. In these multi-dimensional architectures, MXene and graphene sheets establish an electrically conductive, flexible carbon backbone. Intercalated TMO nanoparticles act as physical spacers that suppress sheet restacking, while conductive polymer matrices function as elastic binders that buffer volumetric strain and contribute additional pseudocapacitance. This review examines the design, synthesis, interfacial kinetics, and performance of hybrid electrodes for high-energy-density supercapattery systems (Abbas et al., 2020).

2. Fundamental Properties and Synergistic Roles of Component Nanomaterials

2.1 Transition Metal Oxides (TMOs)

Transition metal oxides ($NiCo_2O_4$, MnO_2, Fe_3O_4, ZnO, $CuCo_2O_4$) serve as primary battery-type redox species in hybrid electrodes, offering multiple oxidation states and high theoretical specific capacities (> 1000 C g^{-1} or F g^{-1}). Charge storage in TMOs proceeds via multi-

electron Faradaic redox reactions involving cation insertion and surface oxidation state changes:

$$MO + C^+ + e^- \rightleftharpoons MOC$$

where M represents the transition metal ion and C^+ denotes the electrolyte cation (H^+, Li^+, Na^+, or K^+) (Liang et al., 2021). Despite their high capacity, standalone TMO electrodes exhibit low intrinsic electrical conductivity and large charge transfer resistance. Volumetric expansion and contraction during Faradaic cycling can cause particle pulverization, loss of electrical contact, and rapid capacity fading (Azadmanjiri et al., 2018).

2.2 Two-Dimensional MXenes ($Ti_3C_2T_x$)

MXenes are produced by selectively etching the "A" atomic layers from parent MAX phases using fluoride-containing etchants. Represented by the general formula $M_{n+1}X_nT_x$ (where M is an early transition metal, X is carbon/nitrogen, and T_x represents surface terminations like $-O$, $-OH$, $-F$, $-Cl$), MXenes combine metallic electrical conductivity (2.4×10^4 S cm^{-1}) with hydrophilic surfaces (Gogotsi & Huang, 2021).

Unlike non-polar carbon substrates, the hydrophilic surface terminations of MXenes enhance electrolyte wetting and ion access to active sub-nanometer channels. Charge storage in MXenes occurs through intercalation pseudocapacitance, where cations reversibly intercalate between conductive layers with minimal structural deformation. However, face-to-face sheet restacking driven by interlayer Van der Waals interactions can restrict ion transport and lower accessible surface area during prolonged operation (Zhu et al., 2021).

2.3 Graphene and Derivatives (rGO)

Graphene and reduced graphene oxide (rGO) provide high theoretical specific surface area (2630 m^2 g^{-1}), mechanical strength, and high electrical conductivity (10^6 S cm^{-1}). Within multi-component hybrid electrodes, graphene acts as a conductive skeletal matrix and flexible current collector (Su & Loh, 2013). Pure graphene stores charge via non-Faradaic electrostatic double-layer formation, while rGO retains oxygen functional groups ($-COOH$, $-OH$) that impart localized pseudocapacitance and improve interfacial wettability. When combined with MXenes, flexible rGO sheets interweave between carbide layers, forming a porous 2D/2D carbon network that accommodates volumetric strain and prevents active material detachment (Li et al., 2022).

2.4 Conductive Polymers (PANI, PEDOT:PSS, PPy)

Conductive polymers, such as polyaniline (PANI) and poly(3,4-ethylenedioxythiophene):polystyrene sulfonate (PEDOT:PSS), provide high mass-specific pseudocapacitance, flexibility, and low density (Rout, 2021). Charge storage in PANI proceeds through reversible doping/dedoping Faradaic processes along its conjugated backbone, cycling between oxidation states (leucoemeraldine, emeraldine, and pernigraniline):

$$PANI^0 + xA^- \rightleftharpoons PANI^x(A^-)_x + xe^-$$

where A^- represents the dopant anion (Guo & Ma, 2018). Standalone conductive polymers degrade during long-term cycling due to mechanical fatigue from counter-ion insertion and extraction. Hybridizing CPs with rigid 2D MXenes or graphene substrates constrains polymer expansion. Strong π-π interactions and hydrogen bonding anchor the polymer chains, maintaining structural integrity over extended charge-discharge cycles (El-Bery et al., 2021).

2.5 Synergistic Multi-Component Integration

Integrating TMOs, MXenes, graphene, and CPs into a single electrode architecture creates synergistic effects across dimensions:

- 2D/2D MXene/graphene networks form a continuous electronic matrix that lowers bulk internal resistance (R_s) and charge transfer resistance (R_{ct}) (Kang et al., 2026).
- Zero-dimensional (0D) or one-dimensional (1D) TMO nanostructures intercalated between 2D sheets act as physical pillars, preventing sheet restacking and creating mesoporous channels for rapid electrolyte transport.
- Interpenetrating conductive polymer networks encapsulate TMO particles, acting as a flexible buffer against volume changes during redox cycling while adding redox active sites (Zhou et al., 2026).

3. Interfacial Engineering and Multi-Component Synthesis Strategies

Synthesizing multi-component nanocomposite electrodes requires control over material distribution, interfacial adhesion, and porous architecture. Physical mixing of individual components often leads to non-uniform phase separation and high contact resistance. Advanced fabrication routes leverage chemical self-assembly, hydrothermal crystallization, and in-situ polymerization to construct integrated heterostructures (Peng et al., 2025).

Hydrothermal and solvothermal growth strategies enable the direct nucleation of TMO nanoparticles ($NiCo_2O_4$, MnO_2, ZnO) onto functionalized MXene or GO sheets. Oxygen groups (−OH, −O) on MXene/GO act as nucleation centers, ensuring strong chemical bonding and low interfacial charge transfer resistance (Yu et al., 2025). In-situ interfacial polymerization introduces monomers (such as aniline) into aqueous suspensions containing pre-formed TMO/MXene/graphene composites. Electrostatic attraction draws monomers onto negatively charged MXene/GO surfaces, where chemical oxidation yields uniform polymer coatings that interlock the 2D sheets. Self-assembled co-coacervation and vacuum-assisted filtration enable the fabrication of flexible, freestanding, binder-free hybrid films with sandwich-like layered microstructures (Yao et al., 2024).

Table 2: Synthetic Routes, Interfacial Coupling Mechanisms, and Key Structural Features of Representative Hybrid Electrodes

Composite System	Primary Synthesis Method	Interfacial Coupling Mechanism	Key Structural Features	Performance Metrics
MnNiS@MXene	Hydrothermal synthesis	Chemical bonding via sulfur bridging at MXene basal planes	Intercalated sulfide prevents MXene restacking; high active area	C_{sp} = 1189.98 C g^{-1} (1983.3 F g^{-1}) at 2 A g^{-1}
Cu-GO/PANI	In-situ chemical electrodeposition	π-π conjugation & Cu-mediated coordination	Fibrillar PANI wrapped on GO; metal doping increases active site density	C_{sp} = 1953 F g^{-1} at 1 A g^{-1}; E = 43.4 Wh kg^{-1}
rGO/Fe_3O_4/PANI (**rGFP**)	Solvothermal & in-situ polymer wrapping	Hydrogen bonding & electrostatic anchoring between PANI and rGO	3D interpenetrating matrix with embedded Fe_3O_4 nanoparticles	C_{sp} = 283.4 F g^{-1}; E = 47.7 Wh kg^{-1} at 550 W kg^{-1}
MXene/PANI/PEDOT:PSS	Wet spinning & in-situ coating	Electrostatic assembly & polymer chain entanglement	Highly conductive fiber matrix; sheet resistance = 0.3 kΩ/sq	C_{sp} = 279 F g^{-1} at 5 mV s^{-1}; R_s = 27.19 Ω
MXene-pBOA-NiO-rGO	Multi-step hydrothermal &	Covalent bridging & interfacial	Expanded gallery spacing; open	C_{sp} = 338.4 F g^{-1};

	polymer intercalation	hydrogen bonding	mesoporous ion channels	$E =$ 16.9 Wh kg^{-1}
$Ti_3C_2T_x$ MXene@ZnO	Chemical precipitation	Surface nucleation at $-O/-OH$ termination sites	Metal oxide spacers prevent restacking; surface area $=$ 43.64 m^2 g^{-1}	$C_{sp} =$ 139.0 F g^{-1}; discharge time $=$ 172.6 s
PANI/Fe_2S_2/MnO_2	Wet chemical polymerization	Synergistic redox bridging in an interpenetrating matrix	Reticular porous fiber network; short diffusion path	$C_{sp} =$ 580 F g^{-1} at 1 A g^{-1}; $E =$ 37.93 Wh kg^{-1}
PANI-COF/NrGO	Condensation & oxidative polymerization	COF integration with conjugated rGO framework	Ordered 3D porous channels with abundant active nitrogen sites	$Q_s =$ 410 C g^{-1} at 2 A g^{-1}; cell $E =$ 9.2 Wh kg^{-1}

4. Electrochemical Performance Metrics and Energy Storage Mechanisms

4.1 Governing Electrochemical Equations

Evaluating supercapattery electrode materials requires separating non-Faradaic capacitive, surface pseudocapacitive, and bulk Faradaic battery-type responses (Franco et al., 2015).

1. **Gravimetric Specific Capacitance (C_{sp}) and Specific Capacity (Q_s):**

Calculated from Galvanostatic Charge-Discharge (GCD) data:

$$C_{sp} = \frac{I \cdot \Delta t}{m \cdot \Delta V} \quad (\text{F g}^{-1})$$

$$Q_s = \frac{I \cdot \Delta t}{m} \quad (\text{C g}^{-1} \text{ or mAh g}^{-1})$$

where I is the discharge current (A), Δt is the discharge time (s), m is the active material mass (g), and ΔV is the operational voltage window (V) (Rajeh et al., 2026).

Calculated from Cyclic Voltammetry (CV) data:

$$C_{sp} = \frac{\int I \, dV}{m \cdot s \cdot \Delta V} \quad (\text{F g}^{-1})$$

where $\int I \, dV$ is the integrated area of the CV curve and s is the scan rate (V s^{-1}).

2. **Specific Energy Density (E):**

$$E = \frac{1}{2} C_{sp} (\Delta V)^2 = \frac{Q_s \cdot \Delta V}{2 \cdot 3.6} \quad (\text{Wh kg}^{-1})$$

where ΔV represents the full cell voltage window (Yang et al., 2018).

3. **Specific Power Density (P):**

$$P = \frac{E}{\Delta t} \times 3600 = \frac{I \cdot \Delta V}{2m} \quad (\text{W kg}^{-1})$$

4. **Coulombic Efficiency (η):**

$$\eta = \frac{\Delta t_{\text{discharge}}}{\Delta t_{\text{charge}}} \times 100\%$$

4.2 Power-Law Kinetic Analysis

The charge storage kinetics of hybrid electrodes can be evaluated using the power-law relationship between peak current (i) and scan rate (v) in cyclic voltammetry experiments:

$$i = av^b \quad \Rightarrow \quad \log(i) = \log(a) + b \log(v)$$

where a and b are empirical parameters (Bernstein, 2026).

- $b = 1.0$: Indicates ideal non-Faradaic capacitive or fast surface pseudocapacitive kinetics governed by charge adsorption/desorption.
- $b = 0.5$: Represents a semi-infinite diffusion-controlled Faradaic battery-type process (Hernandez et al., 2019).

Multi-component hybrid electrodes typically exhibit transitional b-values between 0.7 and 0.9, confirming a hybrid charge storage mechanism. In these structures, the highly conductive MXene and graphene networks enable fast electron transport ($b \rightarrow 1.0$), while embedded TMOs and conductive polymers provide high Faradaic capacity ($b \rightarrow 0.5$) (Talabis et al., 2018).

Table 3: Comparative Electrochemical Performance Metrics of Advanced Multi-Component Supercapattery Electrodes and Devices

Electrode / Device Configuration	Positive / Negative Pair	Electrolyte	Specific Capacity / Capacitance	Cell Voltage (ΔV)	Max Energy Density (E)	Max Power Density (P)	Retention & Cycle Life
MnNiS@MXene//A	MnNiS@MXene // Activated Carbon	1.0 M KOH	307.18 C at 2 A g^{-1}	1.6 V	34.79 Wh k	1142.61 W k	87.57% after 7,000 cycles
Cu-GO/PANI (3-electrode)	Cu-GO/PANI // Pt	1.0 M H_2S	1953 F g^{-} at 1 A g^{-1}	0.45 V	43.40 Wh k	~ 850 W kg^{-}	53.00% after 200 cycles
rGO/Fe_3O_4/ PANI (Solid-state)	rGFP // rGFP	Gel / Solid	283.40 F g at 1 A g^{-1}	1.10 V	47.70 Wh k	550.00 W kg	78.00% after 5,000 cycles
MXene/PANI/PED	Hybrid Fiber // pBOA	Aqueous	279.00 F g at 5 mV s^{-1}	1.4 V	13.00 Wh k	> 1000 W kg	> 90.00% after 10,000 cycles
MXene-pBOA-NiO-	Quaternary Con // AC	Gel / Aqueous	338.40 F g	1.5 V	16.90 Wh k	~ 750 W kg^{-}	Stable over extended cycling
PANI/Fe_2S_2 /MnO_2//AC	PANI/Fe_2S_2/ MnO_2 // AC	Aqueous	580.00 F g at 1 A g^{-1}	1.6 V	37.93 Wh k	850.00 W kg	82.00% after 5,000 cycles
PANI-COF/NrGO	PANI-COF/NrC // Carbon	Aqueous	410.00 C at 2 A g^{-1}	1.2 V	9.20 Wh kg	300.00 W kg	60.00% after 5,000 cycles
NiO-CNT//AC	NiO-CNT // Activated Carbon	1.0 M Na_2	197.70 F g at 2 mV s^{-1}	1.8 V	85.70 Wh k	11200.00 W	91.00% after 4,000 cycles
$K_{0.5}Mn_2O_4$@C//Z	NCMO // Porous Carbon	1.0 M Na_2	75.00 F g^{-} at 10 A g^{-1}	2.4 V	60.00 Wh k	12300.00 W	92.60% after 10,000 cycles

5. System-Level Integration and Supercapattery Device Architectures

Maximizing the energy density of a supercapattery system requires expanding the operating cell voltage window (ΔV), as energy density increases quadratically with voltage ($E \propto \Delta V^2$). In single-component symmetric supercapacitors using aqueous electrolytes, the cell voltage is thermodynamically limited to ~ 1.0 V due to the water-splitting reaction (hydrogen and oxygen evolution at 1.23 V) (Asrari et al., 2026). Asymmetric supercapatteries overcome this limitation by combining a high-overpotential pseudocapacitive or Faradaic positive electrode (such as MnNiS@MXene or $NiCo_2O_4$/PANI) with a carbonaceous negative electrode (activated carbon or rGO). This configuration extends the operating potential window to 1.6–2.4 V in aqueous media (Kamaraj et al., 2026).

To maintain cell stability and prevent localized overcharging, the total charge (q) stored at the positive ($+$) and negative ($-$) electrodes must be balanced ($q^+ = q^-$):

$$q = m \cdot C_{sp} \cdot \Delta V \quad \Longrightarrow \quad \frac{m^+}{m^-} = \frac{C^- \cdot \Delta V^-}{C^+ \cdot \Delta V^+}$$

where m is the active material mass, C is the gravimetric specific capacitance, and ΔV is the potential range during charging/discharging. Proper charge balancing ensures optimal mass loading and utilization of electroactive sites (Ugwuanyi et al., 2026).

Electrochemical Impedance Spectroscopy (EIS) provides insight into internal charge transport resistance. Nyquist plots for hybrid nanocomposite electrodes typically display a low high-frequency real-axis intercept corresponding to the Equivalent Series Resistance (R_s), a small mid-frequency semicircle reflecting the Charge Transfer Resistance (R_{ct}), and a steep low-frequency line ($> 45°$) indicative of low Warburg ion diffusion resistance (Li et al., 2025).

Incorporating conductive polymers and MXenes into metal oxide matrices significantly lowers internal resistance. For instance, combining MXene with PANI and PEDOT: PSS reduces the bulk series resistance (R_s) from $77.51\ \Omega$ (pristine MXene) to $27.19\ \Omega$, while reducing charge transfer resistance (R_{ct}) from $77.57\ \Omega$ to $28.03\ \Omega$. This drop in internal resistance minimizes ohmic voltage drop (IR drop) during rapid discharge, enabling high power density (> 10 kW kg^{-1}) while maintaining stable operation (Rajendran et al., 2026).

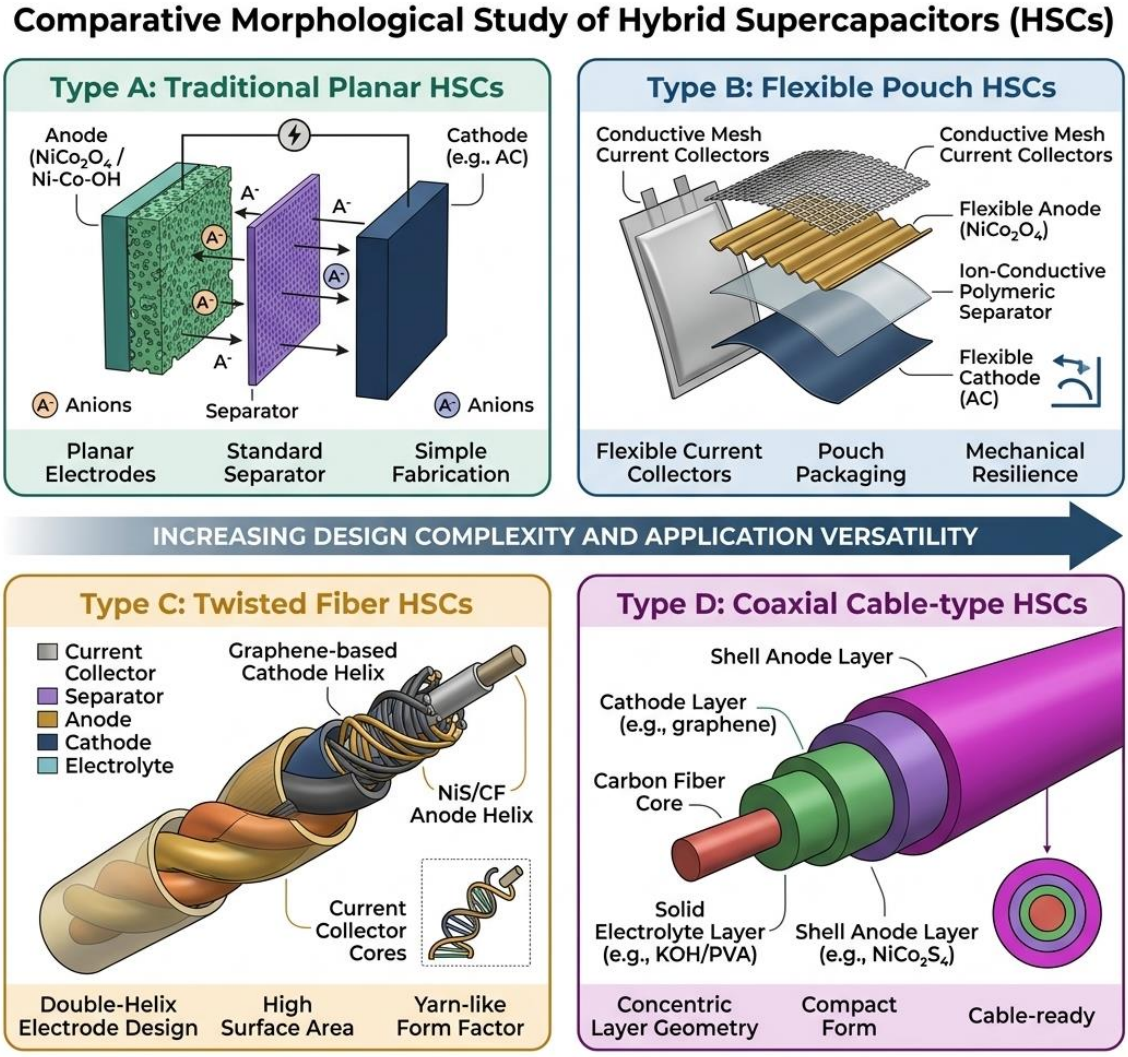


Figure 2. Comparative morphological designs and geometric configurations of hybrid supercapacitors (HSCs), ranging from planar cells to flexible pouch, twisted fiber, and coaxial cable-type form factors.

6. Challenges, Emerging Trends, and Future Perspectives

Despite their performance advantages, multi-component hybrid nanocomposite electrodes face several engineering and scaling challenges:

1. **Ambient Oxidation of MXenes**: In aqueous electrolytes containing dissolved oxygen, titanium-based MXenes ($Ti_3C_2T_x$) can undergo oxidation, forming insulating TiO_2 nanocrystals along sheet edges. This structural degradation degrades electrical conductivity and accelerates capacity loss over time (Samala et al., 2024)).

2. **Interfacial Delamination and Mechanical Strain**: Differing volumetric expansion rates among rigid TMOs, flexible 2D carbon sheets, and swollen conductive polymers can cause mechanical strain during long-term cycling. This strain can lead to phase separation, delamination, and electrical isolation of active particles (Çakmakçı et al., 2024).

3. **Synthesis Complexity and Processing Costs**: Multi-step fabrication procedures involving hydrofluoric acid (HF) etching of MAX phases, solvothermal crystallization, and precise chemical polymerization add processing complexity and

safety requirements that hinder large-scale manufacturing (Uddin et al., 2023).

To address these challenges, several advanced material strategies are under investigation:

- **High-Entropy and Ordered Double-Transition-Metal MXenes**: Utilizing double-transition-metal MXenes (e.g., Mo_2TiC_2) or multi-element high-entropy formulations increases structural stability, broadens electroactive redox states, and improves oxidation resistance compared to conventional $Ti_3C_2T_x$ (Lopes et al., 2020).
- **3D Macroscopic Aerogel and Hydrogel Architectures**: Assembling 2D MXene and graphene sheets into 3D porous hydrogel/aerogel frameworks prevents face-to-face restacking, increases mass loading per unit area, and facilitates electrolyte access throughout the electrode (Naeem et al., 2021).
- **Covalent Organic Framework (COF) Integration**: Incorporating conjugated COFs into conductive polymer networks introduces structured sub-nanometer pore channels and isolated redox-active sites, stabilizing charge transfer while constraining polymer chain deformation (Sathya et al., 2024).
- **In-Situ Characterization and AI-Driven Design**: Applying operando spectroscopic and microscopic techniques enables real-time monitoring of phase changes, oxidation states, and mechanical strain during charge/discharge cycles. Machine learning models can further accelerate the screening of optimal stoichiometry, surface terminations, and component ratios for multi-component heterostructures (Chandrasekaran, 2016).

Conclusion

This review has systematically examined the design, synthesis, and electrochemical performance of multi-component hybrid nanocomposite electrodes integrating transition metal oxides, MXenes, graphene, and conductive polymers for high-energy-density supercapattery systems. The synergistic integration of these disparate nanoscale building blocks into unified architectures addresses the intrinsic limitations of single-component materials, enabling simultaneous enhancement of energy density, power capability, and cycling stability. Key findings demonstrate that 2D/2D MXene/graphene networks establish continuous electronic matrices that substantially lower internal resistance and charge transfer resistance, while intercalated TMO nanoparticles function as physical spacers that suppress sheet restacking and create mesoporous ion transport channels. Conductive polymer matrices contribute additional pseudocapacitance while serving as elastic buffers against volumetric strain during repeated charge-discharge cycling. The electrochemical performance metrics compiled in this review confirm that optimized hybrid electrodes achieve specific capacities exceeding 1000 C g^{-1} and energy densities approaching 100 Wh kg^{-1} while maintaining power densities above 5000 W kg^{-1}. Power-law kinetic analysis reveals that these multi-component systems exhibit transitional b-values between 0.7 and 0.9, validating the hybrid charge storage mechanism combining fast surface-controlled kinetics with bulk Faradaic contributions. System-level considerations including charge balancing, asymmetric cell configuration, and electrolyte optimization enable operating voltage windows of 1.6–2.4 V in aqueous media, leveraging the quadratic dependence of energy density on cell voltage. Despite these advances, several engineering challenges must be addressed to facilitate commercial translation. Ambient oxidation of MXenes in aqueous electrolytes, interfacial delamination arising from mismatched volumetric expansion rates among components, and synthesis complexity associated with multi-step fabrication procedures represent significant barriers to scalable manufacturing. Emerging strategies including high-entropy and ordered double-transition-metal MXenes, three-dimensional macroscopic aerogel and hydrogel architectures, covalent organic framework integration, and AI-driven materials design offer promising pathways to overcome these limitations. Future research should prioritize operando characterization techniques for real-time monitoring of interfacial phenomena, development of green and scalable synthesis routes, and standardization of performance metrics to enable meaningful cross-

study comparisons. The continued advancement of hybrid nanocomposite electrode architectures holds considerable promise for realizing practical supercapattery devices that meet the demanding requirements of next-generation sustainable energy storage systems.

REFERENCES

Abbas, Q., Mirzaeian, M., Hunt, M. R., Hall, P., & Raza, R. (2020). Current state and future prospects for electrochemical energy storage and conversion systems. *Energies*, *13*(21), 5847.

Afreh, P., Gao, L., Passi, B. J., & Onwuagbu, C. C. (2025). Future energy storage: technologies, management systems, and pathways for sustainable integration. *Academia Green Energy*, *2*(2).

Asrari, A., Pandey, A., LaMarche, C. E., & Kowalski, R. P. (2026). From Renewable Variability to Hybrid Stability: Analytical and Experimental Insights into a Transient Buffering Battery–Supercapacitor Framework in a Lab-Scale PV–Wind Microgrid. *Batteries*, *12*(5), 157.

Azadmanjiri, J., Srivastava, V. K., Kumar, P., Wang, J., & Yu, A. (2018). Graphene-supported 2D transition metal oxide heterostructures. *Journal of Materials Chemistry A*, *6*(28), 13509-13537.

Basirun, W. J., Saeed, I. M., Rahman, M. S., & Mazari, S. A. (2021). Nickel oxides/hydroxides-graphene as hybrid supercapattery nanocomposites for advanced charge storage materials–a review. *Critical Reviews in Solid State and Materials Sciences*, *46*(6), 553-586.

Bernstein, J. B. (2026). Correlation Entropy and Power-Law Kinetics. *Entropy*, *28*(6), 712.

Çakmakçı, S., Polatoğlu, B., & Çakmakçı, R. (2024). Foods of the future: challenges, opportunities, trends, and expectations. *Foods*, *13*(17), 2663.

Chandrasekaran, M. (2016). Emerging trends and future perspectives. *Enzymes in food and beverages processing. CRC Press, Tyler & Francis Group*, 505-516.

Detka, K., & Górecki, K. (2023). Selected technologies of electrochemical energy storage—a review. *Energies*, *16*(13), 5034.

El-Bery, H. M., Salah, M. R., Ahmed, S. M., & Soliman, S. A. (2021). Efficient non-metal based conducting polymers for photocatalytic hydrogen production: Comparative study between polyaniline, polypyrrole and PEDOT. *RSC advances*, *11*(22), 13229-13244.

Franco, A. A., Doublet, M. L., & Bessler, W. G. (Eds.). (2015). *Physical multiscale modeling and numerical simulation of electrochemical devices for energy conversion and storage: from theory to engineering to practice*. Springer.

Gogotsi, Y., & Huang, Q. (2021). MXenes: two-dimensional building blocks for future materials and devices. *ACS nano*, *15*(4), 5775-5780.

Guo, B., & Ma, P. X. (2018). Conducting polymers for tissue engineering. *Biomacromolecules*, *19*(6), 1764.

Gür, T. M. (2018). Review of electrical energy storage technologies, materials and systems: challenges and prospects for large-scale grid storage. *Energy & environmental science*, *11*(10), 2696-2767.

Gusain, M., Ahmed, I., & Zhan, Y. (2021). Conducting polymeric nanocomposite for supercapattery. In *Advances in Supercapacitor and Supercapattery* (pp. 63-91). Elsevier.

Hernandez, B. S., Mendoza, E. R., & Reyes V, A. A. (2019). Fundamental decompositions and multistationarity of power-law kinetic systems. *arXiv preprint arXiv:1908.04593*.

Kamaraj, S., Selvaraj, B., Kandhasamy, M., Kamaraj, I., Kim, S., & Kang, J. (2026). Strategies and Emerging Directions for Next-Generation Zinc-Ion Hybrid Supercapacitors. *Energy Technology*, *14*(9), e70641.

Kang, X., Wang, Y., Chen, C., Liu, J., Zhai, X., Niu, C., ... & Li, J. (2026). MXene-based multi-component conductive hydrogel with synergistic crosslinking networks for high-performance wearable sensors. *Nanoscale*, *18*(9), 4874-4886.

Li, C., Zheng, C., Cao, F., Zhang, Y., & Xia, X. (2022). The Development Trend of Graphene Derivatives: C. Li et al. *Journal of Electronic Materials*, *51*(8), 4107-4114.

Li, Z., Yan, X., Tong, R., Zhao, Y., & Lin, D. (2025). Biorefinery inspired biopolymers for green energy storage electronics: structuring and chemical modification to empower their specific functionalization. *Science China Technological Sciences*, *68*(11), 2110501.

Liang, R., Du, Y., Xiao, P., Cheng, J., Yuan, S., Chen, Y., ... & Chen, J. (2021). Transition metal oxide electrode materials for supercapacitors: a review of recent developments. *Nanomaterials*, *11*(5), 1248.

Lopes, J. A. P., Madureira, A. G., Matos, M., Bessa, R. J., Monteiro, V., Afonso, J. L., ... & Magalhães, P. (2020). The future of power systems: Challenges, trends, and upcoming paradigms. *Wiley Interdisciplinary Reviews: Energy and Environment*, *9*(3), e368.

Márquez, J. M. A., Manzano, F. S., & Luengo, J. R. (2023). *Energy storage systems: Fundamentals, classification and a technical comparative*. Springer Nature.

Naeem, M., Jamal, T., Diaz-Martinez, J., Butt, S. A., Montesano, N., Tariq, M. I., ... & De-La-Hoz-Valdiris, E. (2021, November). Trends and future perspective challenges in big data. In *Advances in intelligent data analysis and applications: Proceeding of the sixth euro-China conference on intelligent data analysis and applications, 15–18 October 2019, Arad, Romania* (pp. 309-325). Singapore: Springer Singapore.

Peng, Y., Liu, J., Feng, Z., Peng, J., Guo, Y., Zhang, Y., ... & Deng, L. (2025). Multi-component heterogeneous interface engineering and magnetic domain evolution for broadband electromagnetic wave attenuation. *Chemical Engineering Journal*, 168991.

Priyadharshini, A., Vinodhini, S. P., & Xavier, J. R. (2026). A comprehensive review of graphene-based nanocomposites for high-performance energy storage: advances in design, electrochemical mechanisms, and future prospects. *Ionics*, *32*(3), 2483-2520.

Rajeh, S. Y., Arshad, M., Fahmy, Y. M., Shahbaz, M. A. H., Alomar, M., Amari, A., ... & Afzal, A. M. (2026). Lithium argyrodite@ lithium titanium phosphate@ reduced graphene oxide coated carbon cloth as energy storage and hydrogen evolution reaction electrodes. *Materials Chemistry and Physics*, 132229.

Rajendran, J., Wilson Sukumari, N., & Rajendran, M. (2026). Wearable, Self-Powered Electronic Devices: Logical Framework for Transforming the Future of Digital Health. *Journal of Low Power Electronics and Applications*, *16*(2), 20.

Rout, C. S. (2021). Conducting polymers: a comprehensive review on recent advances in synthesis, properties and applications. *RSC advances*, *11*(10), 5659-5697.

Khan, S. A., Khan, F. A., Jamil, A., & Hameed, A. A. (2024, April). Interpretable motor sound classification for enhanced fault detection leveraging explainable AI. In *2024 IEEE 3rd International Conference on Computing and Machine Intelligence (ICMI)* (pp. 1-10). IEEE.

Khan, F. A., Jamil, A., Khan, S. A., & Hameed, A. A. (2024). Enhancing robotic manipulator fault detection with advanced machine learning techniques. *Engineering Research Express*, *6*(2), 025204.

Samala, A. D., Rawas, S., Criollo-C, S., Bojic, L., Prasetya, F., Ranuharja, F., & Marta, R. (2024). Emerging technologies for global education: A comprehensive exploration of trends, innovations, challenges, and future horizons. *SN Computer Science*, *5*(8), 1175.

Sathya, U., Hashini, S., Lakshmipriya, C., Varun, C. M., & Nalini, M. (2024, December). Emerging Trends and Future Prospects in Internet of Things (IoT) Technology. In *2024 International Conference on Sustainable Communication Networks and Application (ICSCNA)* (pp. 79-85). IEEE.

Solyali, D., Safaei, B., Zargar, O., & Aytac, G. (2022). A comprehensive state-of-the-art review of electrochemical battery storage systems for power grids. *International Journal of Energy Research*, *46*(13), 17786-17812.

Su, C., & Loh, K. P. (2013). Carbocatalysts: graphene oxide and its derivatives. *Accounts of chemical research*, *46*(10), 2275-2285.

Mehmood, A. (2023). Data-driven decision-making in local and global markets: The role of market research in pricing, branding, and distribution strategies. *Pakistan Social Sciences Review*, *7*(3), 1225-1235.

Duhis, M., Mehmood, A., Ahmed, A., & Lawa, A. (2025). Sustainable Development in the Face of Climate Change Integration Climate Mitigation and Adaptation into Urban Planning. *The Critical Review of Social Sciences Studies*, *3*(1), 2377-2390.

Mehmood, A. (2025). Transformational leadership and gender diversity: A mixedmethods study on the effectiveness of women in US Fortune 500 companies. *The American Journal of Management and Economics Innovations*, *7*(3), 30-38.

Mehmood, A., Siddiqui, H. A., & Rashid, M. (2025). Mentorship as a catalyst for leadership development: Strategies, outcomes, and implications for emerging leaders in organizational contexts. *Social Science Review Archives*, *3*(1), 2516-2525.

Talabis, D. A. S., Arceo, C. P. P., & Mendoza, E. R. (2018). Positive equilibria of a class of power-law kinetics. *Journal of Mathematical Chemistry*, *56*(2), 358-394.

Uddin, M., Manickam, S., Ullah, H., Obaidat, M., & Dandoush, A. (2023). Unveiling the metaverse: Exploring emerging trends, multifaceted perspectives, and future challenges. *IEEE access*, *11*, 87087-87103.

Ugwuanyi, S. E., Mgbadike, C. D., Anie, N. O., Onogwu, A. J., Otache, O., Ogbo, M. O., ... & Ugwuanyi, I. C. (2026). Energy Sustainability via Integrated Photovoltaic Solar Cells and Supercapacitors: A Comprehensive Review. *Nigerian Journal of Physics*, *35*(2), 197-206.

Yang, Z., Qiu, A., Ma, J., & Chen, M. (2018). Conducting α-Fe2O3 nanorod/polyaniline/CNT gel framework for high performance anodes towards supercapacitors. *Composites Science and Technology*, *156*, 231-237.

Yao, R., Zhao, H., Yu, F., Zhang, W., Yan, G., Li, Y., ... & Li, Y. (2024). Interfacial engineering of Ni/WC heterostructure electrocatalyst for highly efficient hydrogen evolution reaction in all pH electrolyte. *Journal of Alloys and Compounds*, *972*, 172827.

Yu, W., Zhang, C., Wang, Y., Yang, Z., Wang, Y., Du, H., ... & Xu, Y. (2025). Enhancing structural integrity and performance of Li-Rich Mn-based cathode materials via multi-component surface engineering. *Electrochimica Acta*, 147107.

Zhou, Q., Song, L., Song, M., Lu, L., Pan, W., He, X., ... & Xiong, C. (2026). High-performance multi-component synergistic hydrogel electrolyte with enhanced ion transport for flexible zinc–air batteries and wearable sensors. *Green Chemistry*, *28*(7), 3328-3340.

Zhu, Q., Li, J., Simon, P., & Xu, B. (2021). Two-dimensional MXenes for electrochemical capacitor applications: Progress, challenges and perspectives. *Energy Storage Materials*, *35*, 630-660.